Appendix A
Transverse Broadening Corrections

In Sect. 2.2.2 we discussed the corrections due to transverse interactions derived from a variational approach [1]. Here, we will show the full perturbative expansion for a single gas going up to third order. The calculation closely follows the approach of Mora and Castin [2] and takes the discretization necessary for the definition of the phase operator into account.

From the expression for the width of the transverse wave function we can calculate the mean field interaction energy term for the effective longitudinal Hamiltonian to be

$$E_{\text{int}} = \hbar\omega_\perp\sqrt{1+2a_s n_{1\text{d}}}\ .$$

Requantizing this result and inserting it in the a discretized form of the Hamiltonian introduced in [3] we obtain

$$\hat{H} = \sum_z l\ \hat{\psi}_z^\dagger\Big[-\frac{\hbar^2}{2m}\Delta_z + U_z - \mu + \hbar\omega_\perp\sqrt{1+2a_s\hat{\psi}_z^\dagger\hat{\psi}_z}\Big]\hat{\psi}_z\ .$$

Here, z is the index of position on the grid and l is the dicretization length. We insert a phase-density representation of the field operator on each grid point $\hat{\psi}_z = e^{i\hat{\theta}_z}\sqrt{\hat{n}_z} = e^{i\hat{\theta}_z}\sqrt{n_{1\text{d}}+\delta\hat{n}_z}$ and perturbativly expand the Hamiltonian around small density and long range phase fluctuations. The spatial indices of the fields will be omitted from now on for clarity.

Our interest lies in the modifications the broadening causes in the potential energy terms. Inserting the phase-density representation we obtain

$$\begin{aligned}\hat{H}_p &= \sum_z l\left[(U-\mu)\hat{\psi}^\dagger\hat{\psi} + \hbar\omega_\perp\hat{\psi}^\dagger\sqrt{1+2a_s\hat{\psi}^\dagger\hat{\psi}}\hat{\psi}\right]\\ &= \sum_z l\,\hat{n}\left[(U-\mu) + \hbar\omega_\perp\sqrt{1+2a_s\Big(\hat{n}-\frac{1}{l}\Big)}\right].\end{aligned} \tag{A.1}$$

B. Rauer, *Non-Equilibrium Dynamics Beyond Dephasing*,
Springer Theses, https://doi.org/10.1007/978-3-030-18236-6

Here we used the identity $\hat{\psi}^\dagger\hat{\psi} = \hat{n}$ and the commutator of the field operators $[\hat{\psi}_z,\ \hat{\psi}^\dagger_{z'}] = \frac{\delta_{z,z'}}{l}$. Expanding the square root in this expression for small $a_s\hat{n}$ we can rewrite Eq. (A.1) as

$$\hat{H}_p = \sum_z l\,(n_{1\mathrm{d}} + \delta\hat{n})\left[(U-\mu) + \hbar\omega_\perp\left(1 + a_s\left(n_{1\mathrm{d}} + \delta\hat{n} - \frac{1}{l}\right) - \frac{1}{2}a_s^2\left(n_{1\mathrm{d}} + \delta\hat{n} - \frac{1}{l}\right)^2 + \dots\right)\right].$$

Collecting all terms of order $O(\delta\hat{n}^n)$ with $n \leq 3$, considering that $1/l$ is of second order and associating the obtained series with closed expressions we obtain[1]

$$\begin{aligned}
\hat{H}_p^{(0)} &= \sum_z l\, n_{1\mathrm{d}}\left[(U-\mu) + \hbar\omega_\perp\sqrt{1+2a_s n_{1\mathrm{d}}}\right]\\
\hat{H}_p^{(1)} &= \sum_z l\,\delta\hat{n}\left[(U-\mu) + \hbar\omega_\perp\frac{1+3a_s n_{1\mathrm{d}}}{\sqrt{1+2a_s n_{1\mathrm{d}}}}\right]\\
\hat{H}_p^{(2)} &= \sum_z l\,\delta\hat{n}^2\,\frac{\hbar\omega_\perp a_s}{2}\left[\frac{2+3a_s n_{1\mathrm{d}}}{(1+2a_s n_{1\mathrm{d}})^{3/2}}\right] - \sum_z \frac{\hbar\omega_\perp a_s n_{1\mathrm{d}}}{\sqrt{1+2a_s n_{1\mathrm{d}}}}\\
\hat{H}_p^{(3)} &= -\sum_z l\,\delta\hat{n}^3\,\frac{\hbar\omega_\perp a_s^2}{2}\left[\frac{2a_s^2 n_{1\mathrm{d}}^2 - a_s n_{1\mathrm{d}} + 1}{(1+2a_s^2 n_{1\mathrm{d}}^2)^{5/4}}\right] -\\
&\quad - \sum_t \delta\hat{n}\,\hbar\omega_\perp a_s\left[\frac{2a_s^2 n_{1\mathrm{d}}^2 - a_s n_{1\mathrm{d}} + 1}{(1+2a_s^2 n_{1\mathrm{d}}^2)^{3/2}}\right].
\end{aligned} \tag{A.2}$$

In zeroth order we regain the broadened potential energy for the average density profile $n_{1\mathrm{d}}$. In first order we obtain the broadened expression for the chemical potential given in Eq. (2.33). Therefore, as in the unbroadened case, $H^{(1)}$ vanishes for the density profile that minimizes $H^{(0)}$, i.e. solves the non-polynomial GPE in Eq. (2.34). This again leaves the leading terms governing the fluctuations to be of second order. They are of the same form as in the purely 1d case but their prefactors exhibit a more complicated density dependence. The first term in $H_p^{(2)}$ reproduces g_n defined in Eq. (2.35) and thereby confirms the expression for the speed of sound found from the hydrodynamics relation.

In third order, apart from the rescaled prefactor of the last term in Eq. (A.2) which is also appears in the purely 1d case, the first new term arises. It is proportional to $\delta\hat{n}^3$ and represents the lowest order integrability breaking that arises from the broadening. Combining this term with the second order term, neglecting the last term in Eq. (A.2) and disregarding the constant energy functional in $H_p^{(2)}$ we end up with

$$\hat{H}_p^{(2+3)} = \sum_z l\,\frac{g_n}{2}\delta\hat{n}^2\left(1 - \chi_n a_s\delta\hat{n}\right)\ ,$$

[1]The closed expressions were obtained through the Mathematica function 'FindGeneratingFunction'.

where $\chi_n \approx 1/2$ for $a_s n_{1d} < 1$. As $a_s \delta\hat{n}$ is small, this correction will not have large effects on equilibrium states. For long time dynamics like the loss of coherence observed in the measurements presented in Chap. 5 in might play a larger role. However, as discussed in Sect. 2.2.3, a more rigorous treatment of the integrability breaking effects stemming from transverse interactions performed in Refs. [3, 4] concluded that also the effects on intermediate time dynamics are negligible for our parameter range.

References

1. Salasnich L, Parola A, Reatto L (2002) Effective wave equations for the dynamics of cigar-shaped and disk-shaped Bose condensates. Phys Rev A 65:043614
2. Mora C, Castin Y (2003) Extension of Bogoliubov theory to quasicondensates. Phys Rev A 67:053615
3. Mazets IE, Schumm T, Schmiedmayer J (2008) Breakdown of integrability in a quasi-1D ultracold bosonic gas. Phys Rev Lett 100:210403
4. Mazets IE, Schmiedmayer J (2010) Thermalization in a quasi-one-dimensional ultracold bosonic gas. New J Phys 12:055023

Appendix B
Radial GPE Simulations

Solving the GPE numerically in more than one dimension can become computationally demanding especially when interested in dynamical effects. However, in certain cases the exploitation of symmetries can cast the problem into a lower dimensional form. In this appendix, we will discuss how the 2d GPE can be solved numerically for a radially symmetric problem with the aid of Fourier-Bessel series. The approach maps the 2d problem onto a 1d radial problem thereby significantly reducing the its computational demands.

For an arbitrary potential $U(r)$ the radially symmetric 2d GPE can be written as

$$i\hbar\frac{\partial}{\partial t}\phi(r,t) = -\frac{\hbar^2}{2m}\Delta_r\,\phi(r,t) + U(r)\,\phi(r,t) + g|\phi(r,t)|^2\,\phi(r,t)\ , \tag{B.1}$$

with $r^2 = x^2 + y^2$ and $\Delta_r = \frac{1}{r}\frac{\partial}{\partial r}r\frac{\partial}{\partial r}$ being the radial part of the Laplace operator in polar coordinates. A common strategy to numerically solve the GPE is the split-step method [1]. There, the wave function is propagated alternatingly by the kinetic term of the Hamiltonian and the terms diagonal in real space, using small time steps to minimize the error. The propagation with the kinetic term is usually performed in momentum space where it becomes diagonal. This strategy can also be applied to solve Eq. (B.1), only that instead of obtaining the momentum space wave function through a Fourier transform one uses the Fourier-Bessel series [2], expanding $\phi(r)$ in Bessel functions of the first kind J_α

$$\phi(r) = \sum_{j=1}^{\infty}\psi_j\,J_0(\beta_j\,r)\ , \tag{B.2}$$

$$\psi_j = \frac{2}{\left[L\,J_1(u_{0,j})\right]^2}\int_0^L r\,\mathrm{d}r\ \phi(r)\,J_0(\beta_j\,r)\ . \tag{B.3}$$

Here, $\beta_j = \frac{u_{0,j}}{L}$ are the radial momenta with $u_{0,j}$ being the j-th root of $J_0(r)$ and L the radial size of the system. The pre-factor in front of the integral in Eq. (B.3) is a

B. Rauer, *Non-Equilibrium Dynamics Beyond Dephasing*,
Springer Theses, https://doi.org/10.1007/978-3-030-18236-6

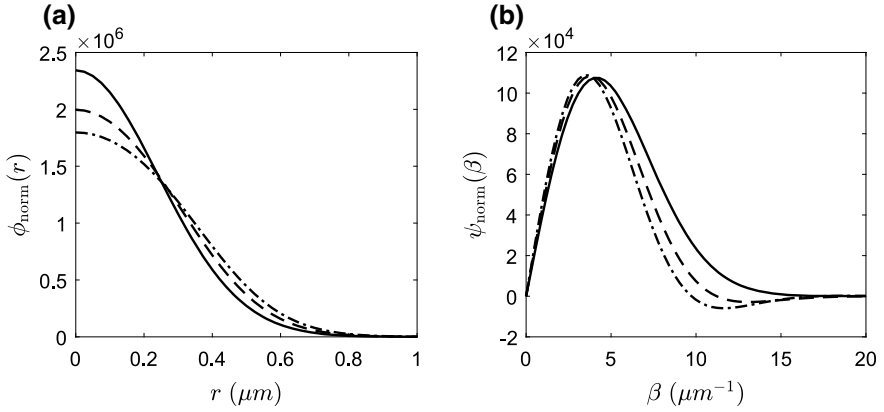

Fig. B.1 Radial wave function. **a** Normalized wave function $\phi_{\mathrm{norm}}(r) = \phi(r)/\sqrt{\int |\phi(r)|^2 r\,\mathrm{d}r}$ of ^{87}Rb atoms trapped in a harmonic confinement with $\omega_\perp = 2\pi \cdot 2$ kHz for three different longitudinal densities $n_{1\mathrm{d}} a_{\mathrm{s}} = 0$, 0.3 and 0.6 (solid, dashed and dash-dotted line). **b** Corresponding Fourier-Bessel coefficients representing the radial momentum distribution

normalization stemming from

$$\int_0^L r\,\mathrm{d}r\ J_0(\beta_i\, r)\, J_0(\beta_j\, r) = \delta_{ij} \frac{\left[L\, J_1(u_{0,j})\right]^2}{2}\ .$$

Using the fact that $J_0(r)$ is a solution of Bessel's differential equation it can be shown that

$$\Delta_r\, \phi(r) = \sum_{j=1}^{\infty} \psi_j\, \Delta_r\, J_0(\beta_j\, r) = -\sum_{j=1}^{\infty} \psi_j\, \beta_j^2\, J_0(\beta_j\, r)\ ,$$

rendering the kinetic term in Eq. (B.1) diagonal for the momentum space wave function ψ_j. This allows for an effective implementation of the kinetic propagation through the transformations defined in Eqs. (B.2) and (B.3).

As for Cartesian coordinates, the ground state of the system can be found through imaginary time evolution. Figure B.1 shows ground states for different numbers of particles in an harmonic potential. Dynamical solutions of Eq. (B.1) are discussed in the context of the transverse expansion of clouds released from the tight atom chip confinement (see Sect. 3.3.1). It is important to note that this approach is limited to fully radially symmetric problems. For example, dipole oscillations of a condensate trapped in a otherwise radially symmetric potential can not be simulated.

This approach can further be extended to cylindrical coordinates (r, z) to effectively solve 3d problems. There, a combination of Fourier transform and Fourier-Bessel series can be used to obtain the momentum space wave function.

References

1. Bao W, Jaksch D, Markowich PA (2003) Numerical solution of the Gross-Pitaevskii equation for Bose-Einstein condensation. J Comput Phys 187:318–342
2. Kaplan W (2002) Advanced calculus, 5th edn. Pearson

Appendix C
Bootstrap

Bootstrapping is a resampling technique that allows in many cases to assert the accuracy of a parameter estimation even for complex estimators where an accuracy measure (i.e. confidence interval, bias,…) is hard to calculate analytically [1, 2]. Its core premise is to assume the empirical distribution of measured data to be a good approximation of the unknown true distribution underlying the data. From this empirical distribution the statistical quantities are then calculated, generally by resampling the available data with replacement. In the following, first an intuitive example is given before a typical use case from the data analysis presented in this thesis is described.

Let us consider a set of measured data $\{x_1, \ldots, x_n\}$ from which we infer the sample mean, $\bar{x} = \frac{1}{n}\sum_i x_i$. If we want to know how accurate the value is we obtained we can perform a bootstrap. For that, we resample the data with replacement and thereby generate a set of bootstrap samples each containing again n values. Looking at one of these bootstrap samples, some of the original values will most likely appear multiple times and some will not appear at all. Also, the probability that the original sample is reproduced is very small if n is large. From each of these bootstrap samples we can now infer its sample mean, which gives us the bootstrap distribution. This distribution gives a measure of accuracy for the value $\bar{x}$ estimated from the original sample and allows us to obtain confidence intervals. In this simple example one could have also directly calculated the standard error of the mean $\bar{\sigma} = \sqrt{\sum_i (x_i - \bar{x})^2/n(n-1)}$. However, if the estimator of interest is more complicated and such an expression is not known the bootstrap provides a simple technique to infer measures of accuracy.

In this thesis, bootstrapping is used to obtain confidence intervals for parameter estimations which involve correlation functions or fits to features of correlation functions. An example for measured data that is resampled are sets of phase profiles $\{\varphi_1(z), \ldots, \varphi_n(z)\}$, where each spatial profile $\varphi_i(z) = [\varphi_i(z_1), \varphi_i(z_2), \ldots, \varphi_i(z_m)]$ is a vector extracted from a single interference picture (see Sect. 3.3.4). Here, m is the number of pixels for which the phase is extracted and z_j are the positions in the cloud corresponding to the individual pixels. Typically, like in the recurrence measurements presented in Chap. 5, multiple of these phase profile sets are taken at different evolution times t. Let us now consider the case of the recurrence height

B. Rauer, *Non-Equilibrium Dynamics Beyond Dephasing*,
Springer Theses, https://doi.org/10.1007/978-3-030-18236-6

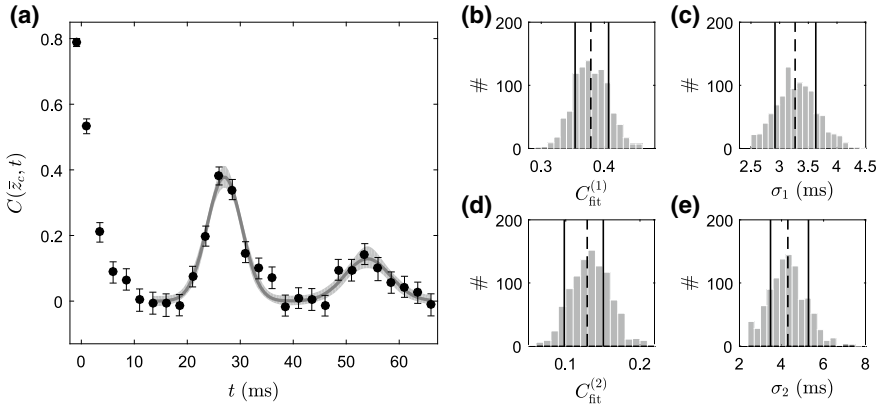

Fig. C.1 Bootstrap example. **a** Fit of the recurrence height for a system with $T_{\rm eff} = 72$ nK and $L = 49$ µm, presented earlier in Fig. 5.10c. The shaded area shows the fit values between the 10th and the 90th percentile of the bootstrap distribution for 999 runs. The fit function is given in Eq. (5.5). **b**, **d** Corresponding distributions of fitted recurrence heights $C_{\rm fit}^{(1,2)}$ of the first and second recurrence, respectively. The dashed lines indicate the values estimated from the original sample while the solid lines give the obtained 68% confidence intervals. **c**, **e** Same for the recurrence widths $\sigma_{1,2}$

fits presented in Fig. 5.10. There we want to fit a feature in the dynamics of the phase correlation function $C(\bar{z}, t)$ which is calculated from the phase profiles (see Eqs. (2.25) and (5.2)). For that, we draw samples from the full measurement runs, where one run includes one profile from each evolution time.[2] From these samples we calculate the phase correlations and fit the double Gaussian function given in Eq. (5.5) to the spatial cut $C(\bar{z}_c, t)$. Doing this for many resampled configurations, typically around 1000, we obtain a distribution of the fitted recurrence heights $C_{\rm fit}^{(1,2)}$ and recurrence width $\sigma_{1,2}$ (Fig. C.1). From these distributions we can infer confidence intervals which translate, for example, to the confidence intervals of $H_{\rm rec}$ shown in Fig. 5.13. This is done by the bias-corrected and accelerated method [1] implemented by the Matlab function 'bootci'.

References

1. Efron B, Tibshirani R (1986) Bootstrap methods for standard errors, confidence intervals, and other measures of statistical accuracy. J Stat Sci 1:54–75
2. Bohm G, Zech G (2010) Introduction to statistics and data analysis for physicists. Verlag Deutsches Elektronen-Synchrotron

[2]These profiles are independent of each other and therefore could, in principle, also be sampled independently. However, in the current implementation of Matlabs 'bootci' it is not possible to sample from multiple sets.